Contrast agent detection in RF IVUS using one-class cost-sensitive learning

E. Gerardo Mendizabal and Ioannis A. Kakadiaris

Department of Computer Science
University of Houston
Houston, TX, 77204, USA
http://www.cs.uh.edu

Technical Report Number UH-CS-09-08

August 22, 2009

Keywords: IVUS characterization, Vasa vasorum, One class learning, Contrast agent.

Abstract

In this report, we investigate the feasibility of detecting contrast agent in intravascular ultrasound (IVUS) sequences by the characterization of the radio-frequency (RF) signal using one-class cost-sensitive learning. Samples from RF signal corresponding to contrast-free baseline IVUS and contrast agent were acquired and used to compute spectral-based and wavelet-based features over a three-dimensional window of size. The samples were used to compute two contrast detection classifiers (CDC) based on a one-class cost-sensitive support vector machines (SVM) method. For the first contrast detection classifier (CDC_1), we train the one-class SVM to recognize the contrast agent RF signal. For the second contrast detection classifier (CDC_2) we train the SVM to recognize baseline IVUS RF signal and detect the contrast agent by the rejection from this model. The performance of these models was evaluated for frequency-domain and wavelet-based features using different window sizes by computing the rate of the detection of contrast-agent (CD) and the rejection of baseline IVUS (BR) for CDC_1 and the rate of the detection of baseline IVUS (BD) and the rejection of contrast agent (CR) for CDC_2 in two 40MHz IVUS sequences from swine on which a bolus injection of contrast agent (SonoVue®) was employed. Using frequency-domain features, the best average performances for CDC_1 (CD=96.61% and BR=95.67%) and CDC_2 (BD=96.79% and CR=94.24%) were obtained for a window of size: ($r = 255$, $\theta = 7$, $t = 13$). The best performances for wavelet-based features for CDC_1 (CD=96.79% and BR=94.13%) and CDC_2 (BD=98.51% and CR=96.94%) were obtained using the same window size.

Contrast agent detection in RF IVUS using one-class cost-sensitive learning

E. Gerardo Mendizabal and Ioannis A. Kakadiaris

Abstract

In this report, we investigate the feasibility of detecting contrast agent in intravascular ultrasound (IVUS) sequences by the characterization of the radio-frequency (RF) signal using one-class cost-sensitive learning. Samples from RF signal corresponding to contrast-free baseline IVUS and contrast agent were acquired and used to compute spectral-based and wavelet-based features over a three-dimensional window of size. The samples were used to compute two contrast detection classifiers (CDC) based on a one-class cost-sensitive support vector machines (SVM) method. For the first contrast detection classifier (CDC_1), we train the one-class SVM to recognize the contrast agent RF signal. For the second contrast detection classifier (CDC_2) we train the SVM to recognize baseline IVUS RF signal and detect the contrast agent by the rejection from this model. The performance of these models was evaluated for frequency-domain and wavelet-based features using different window sizes by computing the rate of the detection of contrast-agent (CD) and the rejection of baseline IVUS (BR) for CDC_1 and the rate of the detection of baseline IVUS (BD) and the rejection of contrast agent (CR) for CDC_2 in two 40MHz IVUS sequences from swine on which a bolus injection of contrast agent (SonoVue®) was employed. Using frequency-domain features, the best average performances for CDC_1 (CD=96.61% and BR=95.67%) and CDC_2 (BD=96.79% and CR=94.24%) were obtained for a window of size: ($r = 255$, $\theta = 7$, $t = 13$). The best performances for wavelet-based features for CDC_1 (CD=96.79% and BR=94.13%) and CDC_2 (BD=98.51% and CR=96.94%) were obtained using the same window size.

Index Terms

IVUS characterization, Vasa vasorum, One class learning, Contrast agent.

I. Introduction

In the majority of cardiovascular diseases, the acute coronary syndromes are the result of inflammation of the coronary arteries and thrombosis-related complications (i.e., plaque rupture). The vasa vasorum (VV) is a network of microvessels that nourish the tissues of the wall of bigger vessels [1]. Recent studies have related the presence of neovascularization in the vasa vasorum of the plaque as a common feature of inflammation [2] and a preceding or concomitant factor associated with plaque rupture and instability [3], [4]. For this reason, there is an urgent need for tools that allow detection and measurement of plaque neovascularization and detection of leakage and entrapment of blood within atherosclerotic plaques. Such measurements can enable developing an index of plaque vulnerability. Intravascular ultrasound (IVUS) is currently the gold-standard technique for assessing the morphology of blood vessels and atherosclerotic plaques *in vivo*. Although IVUS provides reliable cross section images of the coronary arteries, the *in vivo* imaging of the coronary VV remains a great challenge due to its small size, its echo transparency, and the different IVUS artifacts. To overcome these limitations, IVUS is being used in combination with contrast agents in the form of microbubbles with size similar to red blood cells (RBC). Microbubbles resonate in response to the pressure changes induced by the ultrasound wave. This makes them several times more echogenic than normal body tissues and as result they appear bright in the B-mode ultrasound images. These contrast agents serve as surrogate RBCs and perform acoustically as true intravascular tracers providing, in real-time, the amount and distribution of neovessels within atherosclerotic lesions [5]. In the literature, two methods have been proposed for the detection of microbubbles within the vessel wall. The first method [6], [7], [8] uses differential imaging to quantify the changes in intensity due to microcirculation after the microbubbles' injection. The disadvantage of these methods is related to the necessity of using gated sequences and a registration step. These tasks are difficult due to the nature of the IVUS images. In addition, these methods work with the cartesian B-mode representation. This is a disadvantage because the transformation to this representation results in loss of potentially valuable information. In the second method [9], [10], [11], the harmonic oscillations induced on the microbubbles are detected by a

specially designed IVUS system. The disadvantage of this method is the necessity of a custom-build IVUS system that is not currently commercially available.

In this work, we investigate the feasibility of detecting contrast agent on IVUS sequences by the characterization of the radio frequency (RF) IVUS signal using two contrast detection classifiers (CDC) based on one-class cost-sensitive learning. In the first contrast detection classifier (CDC_1), we build a model for the detection of contrast agent from samples of contrast agent present in the lumen during the microbubble injection. In the second contrast detection classifier (CMC_2), we detect the contrast agent as a change from baseline IVUS (i.e., lumen, intima, media and adventitia signals acquired from frames prior to the bolus injection).

Our contribution is a method for the identification of contrast agent in ungated IVUS data based on one-class cost-sensitive learning using the RF IVUS signal. The primary advantage of this method is that by using the RF IVUS data, we do not lose information contained in the frequency of the signal. The second advantage is that by using one-class learning, we do not need to provide "background" samples for building the classifiers. In our case this is important because, although samples for contrast agent in lumen can be acquired by manual annotations from an expert, the background can consist of a wide variety of other imaged tissues. Thus, obtaining samples for the other tissues may be difficult and labor-intensive to obtain.

II. Previous work

The majority of existing methods for IVUS data analysis are focused on the characterization of atherosclerotic plaque composition [12], [13], [14], [15]. These methods can be divided in two categories: those that extract texture features from the gray-level IVUS B-mode representation [12], [13] and those that analyze the ultrasound RF signal [14], [15]. Since the B-mode images are generated using only the amplitude information of the RF signal, those methods that deal directly with it are expected to provide better results. In fact, it has been shown that the ultrasound RF signals provide quantitative information on tissue microstructures [16], [17].

Nair *et al.*[14], [15] proposed a method known as "virtual histology" (IVUS-VH) that is based on the power spectral analysis (intercept, slope, mid-band fit, and minimum and maximum powers and their corresponding frequencies) of the IVUS RF signals combined with classification trees. High accuracies (>85%) were reported for differentiating fibrous, fibrofatty, calcified, and necrotic regions. In addition, Rodriguez-Granillo and Nasu *et al.* [18], [19], preset *in-vivo* studies of this method reporting high correlation with the corresponding histology. Kawasaki *et al.* [20], [21] proposed another method of tissue classification using the integrated backscatter (IB) that is a parameter derived from the RF signal. The resulting values from this parameter are used to divide the tissue into five categories: thrombus, intimal hyperplasia or lipid core, fibrous tissue, mixed lesions and calcification. This method has demonstrated high sensitivity and specificity for characterizing calcification (100%, 99%), fibrosis (94%, 84%), and lipid pool (84%, 97%) [22]. O'Malley *et al.* [23] presented a study of the feasibility of blood characterization on IVUS data using features intended to quantify speckle and features based on frequency-domain measures of high-frequency signal using one-class support vector machines on the RF raw signal, the signal envelope and the log-compressed signal envelope. Most recently, the feasibility of using wavelet analysis for plaque characterization using the RF amplitude [24], [25] and the RF signal itself [26] has been studied with promising results. Furthermore, wavelet analysis has also been used for blood classification [27] and IVUS image segmentation [28], [29].

III. Methods

Experimental data

In vivo ungated IVUS sequences were acquired in swines using a 40 MHz catheter, from which the raw backscatter data were sampled at 400 MHz. Recordings were made over several minutes, during which time the catheter was held steady. Approximately half-way through the recording session, a bolus injection of microbubbles (SonoVue®) took place proximally to the imaging catheter. This resulted in a brief (1 to 3 *s.*) period of luminal echo-opacity followed by a gradual diminution of contrast in the lumen (5 to 10 *s.*).

A. One-class cost-sensitive learning

The one-class support vector machine (SVM) method is a widely-studied learner or "recognizer". The strategy of one-class SVM is to map the data into an infinite feature space and then use a hyper-sphere to describe the data

in that feature space. The goal is to have the smallest possible hyper-sphere that includes most of the training data. The trade-off between the radius of the hyper-sphere and the number of training samples that it can hold is set by the parameter $\nu \in [0, 1]$. Small values of ν will attempt to put more data into the hyper-sphere while larger values of ν will try to squeeze the size of the hyper-sphere. The second parameter of interest is the width, γ, of the SVM radial basis function (i.e., $k(\mathbf{x}, \mathbf{x}') = \exp(-\gamma \left\|\mathbf{x} - \mathbf{x}'\right\|^2)$ for a pair of feature vectors $\mathbf{x}$ and $\mathbf{x}'$). Properties of a good SVM solution include an acceptable classification rate as well as a low number of resulting support vectors relative to the number of training examples.

B. Features

By stacking the 1-D raw signals we obtain a 2-D frame in polar coordinates. Stacking consecutive frames over time, we obtain a 3-D IVUS signal volume $S(R, \Theta, T)$ (Fig. 1) where R indicates radial distance from the transducer, Θ is the angle with respect to an arbitrary origin, and T is the time since the start of the recording (i.e., frame number).

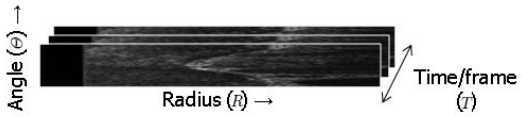

Fig. 1. 3-D IVUS signal volume obtained by frame stacking.

We study the feasibility of characterizing the contrast agent's signal using two types of features: features based on frequency-domain spectral characterization as proposed by O'Malley *et al.* [23] and features based on 2-level 2-D discrete wavelet decomposition. These features are defined for a 3-D window of size $r \times \theta \times t$. The frequency-domain-based features are computed as:

$$f_{\zeta}^{\Gamma}(R, \Theta, T) = \sum_{i=1}^{\lceil r/2 \rceil} \sum_{j=1}^{\lceil \theta/2 \rceil} \sum_{k=1}^{\lceil t/2 \rceil} ijk \hat{W}(i, j, k) \ , \tag{1}$$

$$f_{\eta}^{\Gamma}(R, \Theta, T) = \frac{F_{\zeta}}{\sum_{i=1}^{\lceil r/2 \rceil} \sum_{j=1}^{\lceil \theta/2 \rceil} \sum_{k=1}^{\lceil t/2 \rceil} \hat{W}(i,j,k)} \ , \tag{2}$$

with $\Gamma \in S, E, L$ being S the 3-D signal volume, E the 3-D volume of the signal envelope and L the log-compressed volume of the signal envelope, and $\hat{W}$ defined as the magnitude of the Fourier spectrum of the windowed signal W centered on the point (R,Θ,T).

The wavelet decomposition-based features are computed as:

$$f_{A,l}^{S}(R, \Theta, T) = \sum_{i=1}^{\lceil r \rceil} \sum_{j=1}^{\lceil \theta \rceil} \sum_{k=1}^{\lceil t \rceil} |A_l(W(i, j, k))| \tag{3}$$

$$f_{H,l}^{S}(R, \Theta, T) = \sum_{i=1}^{\lceil r \rceil} \sum_{j=1}^{\lceil \theta \rceil} \sum_{k=1}^{\lceil t \rceil} |H_l(W(i, j, k))| \tag{4}$$

$$f_{V,l}^{S}(R, \Theta, T) = \sum_{i=1}^{\lceil r \rceil} \sum_{j=1}^{\lceil \theta \rceil} \sum_{k=1}^{\lceil t \rceil} |V_l(W(i, j, k))| \tag{5}$$

$$f_{D,l}^{S}(R, \Theta, T) = \sum_{i=1}^{\lceil r \rceil} \sum_{j=1}^{\lceil \theta \rceil} \sum_{k=1}^{\lceil t \rceil} |D_l(W(i, j, k))| \tag{6}$$

where $A_l(\cdot)$, $H_l(\cdot)$, $V_l(\cdot)$ and $D_l(\cdot)$ are the approximation, horizontal detail, vertical detail, and diagonal detail, respectively, at level l of the 2-D discrete wavelet transform decomposition of W.

C. Contrast agent and baseline samples

The contrast agent samples were obtained from a manual segmentation of the lumen by an expert on those frames that encompass the period from when the lumen was no longer echo-opaque following injection to when contrast was no longer visible in the lumen. For obtaining the baseline IVUS samples, we use data from the pre-injection period that corresponds to those frames that encompass the period from the start of the recording to one frame before the contrast agent was first visible in the lumen.

Only those samples for which the class remains constant along the 3-D window are used. The features are computed for this window and are associated with the class contained by it. To improve the scaling of the feature space, each feature of the samples used for training is normalized to zero mean and unit variance. The normalization values are retained for use in testing and deployment.

For the CDC_1, contrast agent samples are used as examples for the positive class S_+ in training and testing. In addition, baseline IVUS samples are used as negative examples S_- for testing, since we know that these samples are contrast agent-free. Similarly, for the CDC_2, samples from the baseline IVUS are used as the positive examples S_+ for training and testing, and samples of contrast agent are used as negative examples S_- for testing the detection of the change.

D. Training

Given a set of positive S_+ and negative S_- examples, a grid search for the one-class SVM parameters γ and ν is performed over a subset of the positive and negative samples to optimize the classifiers. Optimization in this case aims to obtain an acceptable true positive rate on S_+, true negative rate on S_-, and low number of support vectors. The one-class SVM models for the CDCs are computed using only the positive examples of the subset corresponding to each case. Next, the rest of the positive and negative examples are used for testing. Thus, we will have two performances: rate of samples of the class of interest (contrast agent for CDC_1 and baseline IVUS for CDC_2) correctly classified as positive, and rate of other samples correctly classified as negative.

The parameters γ and ν must be selected in such a way that high rate on the classification of both classes is achieved. Therefore, the criteria for the selection of the best parameters is given by a weighted linear combination of the accuracy on the classification of both classes:

$$R = w_1 R_P + w_2 R_N, \tag{7}$$

where R stands for total rate, R_P and R_N are the rates of the class of interest and the negative samples respectively, and w_1 and $w_2 \in [0, 1]$ are the weights associated with the class of interest and negative sample rates respectively. This can be considered cost-sensitive learning for one-class classifiers.

E. Deployment

The performance of the CDCs was evaluated for the frequency-domain and two-level wavelet-based features using two different IVUS sequences. Since the performance of the features is related to the window size (r, θ, t) used for extracting them, we compute the performance of each type of feature separately. We use different sizes of windows on each experiment for each sequence by computing the average rate of detection of contrast-agent (CD) and the rejection of baseline IVUS (BR) for CDC_1 and the rate of the detection of baseline IVUS (BD) and the rejection of contrast agent (CR). For all the experiments, the weights used for the cost-sensitive learning were $w_1 = 0.6$ and $w_2 = 0.4$ for both CDCs.

IV. Results

Tables I and II show the number of contrast agent (CA) and baseline IVUS (BL) samples used for training and testing in each experiment for the first and second sequences, respectively. These samples were used for both CDCs simply by changing the class of importance (CA for the CDC_1 and BL for CDC_2). Tables III and IV show the average performance results when using the frequency-domain and the wavelet-based features, respectively, for both CDC_1 and CDC_2.

The best performance for both CDCs and the two type of features are obtained when using a window of size ($r = 255$, $\theta = 7$, $t = 13$). For the frequency-domain features, the best average performance with CDC_1 is

CD=96.61% and BR=95.67%. With CDC_2 is BD=96.79% and CR=94.24%. The best performance for wavelet-based features with CDC_1 is CD=96.79% and BR=94.13%. With CDC_2 is BD=98.51% and CR=96.94%.

In more detail, the performance of the frequency-domain-based features have a strong dependence on the time information (t), and a moderate dependence on the radial information (r) for both CDCs. The best results for this cases are obtained when using a window size with $r \geq 127$ and $t = 13$ independently of the size of θ. For windows with $t < 13$, the performance reduce rapidly despite the values of r and t. On the other hand, wavelet-based features tend to be more consistent independently of the time, angular and radial information as long as the overall information is sufficient. Here, for CDC_1, the best results are obtained using a window of size $r = 255$ independently of the size of θ and t. However, for CDC_2, wavelet-based features are shown to be more robust to variation on the window size achieving good performance even for the smallest window used in the experiments.

Figures 2 and 3 depict examples of the classification results for CDC_1 using the frequency-domain-based features and wavelet-based features, respectively, on frames corresponding to pre-injection (Fig. 2(a) and Fig. 3(a)) and during-injection (Fig. 2(b) and Fig. 3(b)) with a window of size ($r = 255$, $\theta = 7$, $t = 13$). Most of the misclassifications on the pre-injection frames occur in the lumen. This is due to the fact that the contrast agent samples were acquired from the lumen on the frames corresponding to the microbubble injection where some blood can be still present. However, this does not pose a problem at all since the long-term goal of contrast agent detection is the revelation of angiogenesis in the plaque. Then, we can exclude the lumen from the analysis. The majority of the misclassification of the during-injection frames occurs in places where the radial information r of the corresponding window is near to a change in tissue (i.e., change from lumen to media/adventitia).

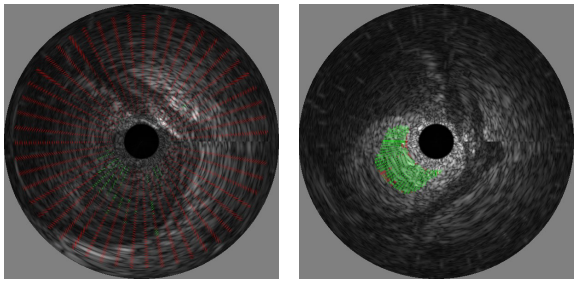

(a) (b)

Fig. 2. Classification results for CDC_1 using the frequency-domain-based features in (a) IVUS frame before injection and (b) IVUS frame during the injection. In both images, the green color indicates the pixels classified as contrast agent and the red color those classified as non-contrast agent.

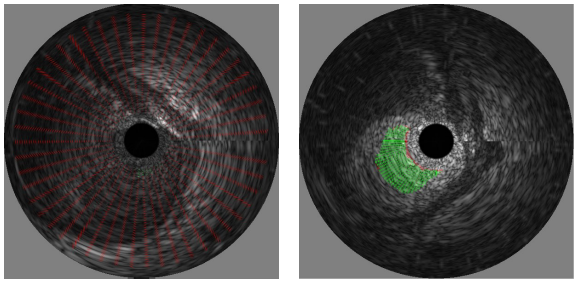

(a) (b)

Fig. 3. Classification results for CDC_1 using the wavelet-based features in (a) IVUS frame before injection and (b) IVUS frame during the injection. In both images, the green color indicates the pixels classified as contrast agent and the red color those classified as non-contrast agent.

Figure 4 depicts an example of the classification results for CDC_2 using the frequency-domain-based features and a window of size ($r = 255$, $\theta = 7$, $t = 13$). In the pre-injection frame (Fig. 4(a)), we can observe that most of the misclassifications do not occur in the lumen as with CDC_1, but in different places along the wall. This is due to the lack of samples that are sufficiently representative of all the different tissues in the vessel. Moreover, in the during-injection frames (Fig. 4(b)) we can observe that most of the contrast agent was detected as a change

from baseline IVUS data, with only some misclassifications of those samples where the radial information r of the corresponding window is near to a change on tissue (i.e., change from lumen to media/adventitia). Regarding the results with CDC_2 and wavelet-based features (Fig. 5), we can observe a better performance for both the pre-injection (Fig. 5(a)) and the during-injection frames (Fig. 5(b)) as expected.

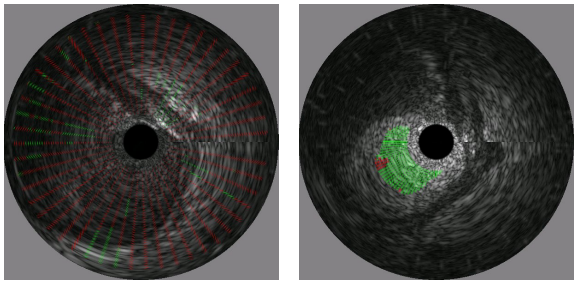

(a) (b)

Fig. 4. Classification results for CDC_2 using the frequency-domain-based features in (a) IVUS frame before injection and (b) IVUS frame during the injection. In both images, the green color indicates the pixels classified as non-baseline and the red color those classified as baseline.

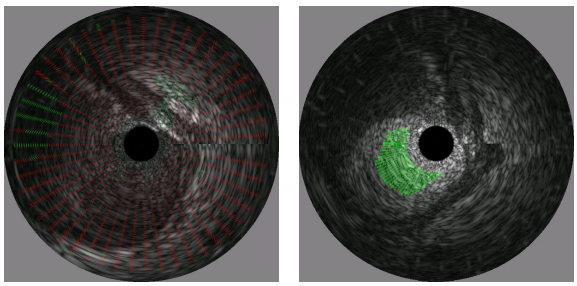

(a) (b)

Fig. 5. Classification results for CDC_2 using the wavelet-based features in (a) IVUS frame before injection and (b) IVUS frame during the injection. In both images, the green color indicates the pixels classified as non-baseline and the red color those classified as baseline.

V. Discussion

The results obtained in our experiments indicate that it is possible to identify contrast agent in IVUS data using one-class learning techniques. In addition, we observe that wavelet-based features perform better and are more robust compared with the frequency-domain-based features.

Since the radius of the hyper-sphere is controlled by the parameter w, cost-sensitive learning is possible with one-class.

Although our method provides promising results without the necessity of gating or a registration step, the inclusion of this pre-process could increase accuracy and would allow us to use a smaller window to achieve higher resolution. Future research includes the use of this preprocessing step and the investigation of new features.

VI. Limitations

For the results presented here, training and testing were performed on each sequence independently. A topic of future investigation is whether a classifier trained on one sequence will have similar accuracy when applied to another (for instance, a sequence recorded from a different subject or even with a different catheter or contrast agent).

To achieve our ultimate goal of detecting and quantifying the microvasculature, it is necessary to increase the resolution of our method.

Histological validation would be necessary to determine the accuracy of our approach when applied to the detection of extra-luminal blood.

VII. Conclusion

We have presented a method for the identification of contrast agent in IVUS with contrast detection models based on one-class cost-sensitive learning. Both approaches have demonstrated the feasibility of detecting contrast agent using the raw IVUS signal without the necessity of a reference image or registration.

References

[1] D. D. Heistad and M. L. Marcus, "Role of vasa vasorum in nourishment of the aorta," *Blood Vessels*, vol. 16, pp. 225–238, 1979.

[2] M. Gossl, N. Malyar, M. Rosol, P. Beighley, and E. Ritman, "Impact of coronary vasa vasorum functional structure on coronary vessel wall perfusion distribution," *American Journal of Physiology - Heart and Circulatory Physiology*, vol. 285, no. 5, pp. H2019–H2026, 2003.

[3] M. Hayden and S. Tyagi, "Vasa vasorum in plaque angiogenesis, metabolic syndrome, type 2 diabetes mellitus, and atherosclerosis: A malignant transformation," *Cardiovascular Diabetology*, vol. 3, no. 1, February 2004.

[4] F. Kolodgie, H. Gold, A. Burke, D. Fowler, H. Kruth, D. Weber, A. Farb, L. Guerrero, M. Hayase, R. Kutys, J. Narula, A. Finn, and R. Virmani, "Intraplaque hemorrhage and progression of coronary atheroma," *New England Journal of Medicine*, vol. 349, no. 24, pp. 2316–2325, December 2003.

[5] J. Granada and S. Feinstein, "Imaging of the vasa vasorum," *Nature Clinical Practice Cardiovascular Medicine*, vol. 5, no. 2s, pp. S18–S25, 2008.

[6] S. O'Malley, S. Carlier, M. Naghavi, and I. Kakadiaris, "Image-based frame gating of IVUS pullbacks: A surrogate for ECG," in *Proc. IEEE International Conference on Acoustics, Speech, and Signal Processing*, Honolulu, HI, 2007, pp. 433–436.

[7] S. M. O'Malley, M. Vavuranakis, M. Naghavi, and I. A. Kakadiaris, "Intravascular ultrasound-based imaging of vasa vasorum for the detection of vulnerable atherosclerotic plaque," in *Proc. 8^{th} Medical Image Computing and Computer-Assisted Intervention, Palm Springs, California, USA*, October 2005, pp. 343–351.

[8] S. Carlier, I. Kakadiaris, N. Dib, M. Vavuranakis, C. Stephanadis, S. O'Malley, C. Hartley, R. Metcalfe, R. Mehran, E. Falk, K. Gul, and M. Naghavi, "Vasa vasorum imaging: A new window to the clinical detection of vulnerable atherosclerotic plaques," *Current Atherosclerosis Reports*, vol. 7, no. 2, pp. 164–169, Mar. 2005.

[9] D. E. Goertz, M. E. Frijlink, N. de Jong, and A. F. van der Steen, "Nonlinear intravascular ultrasound contrast imaging," *Ultrasound in Medicine and Biology*, vol. 32, no. 4, pp. 491–502, 2006.

[10] D. E. Goertz, M. E. Frijlink, D. Tempel, L. C. van Damme, R. Krams, J. A. Schaar, F. J. Ten Cate, P. W. Serruys, N. de Jong, and A. F. van der Steen, "Contrast harmonic intravascular ultrasound: A feasibility study for vasa vasorum imaging," *Investigative Radiology*, vol. 41, no. 8, pp. 631–638, 2006.

[11] D. E. Goertz, M. E. Frijlink, D. Tempel, V. Bhagwandas, A. Gisolf, R. Krams, N. de Jong, and A. F. W. van der Steen, "Subharmonic contrast intravascular ultrasound for vasa vasorum imaging," *Ultrasound in Medicine and Biology*, vol. 33, no. 12, pp. 1859–1872, 2007.

[12] D. Vince, K. Dixon, R. Cothren, and J. Cornhill, "Comparison of texture analysis methods for the characterization of coronary plaques in intravascular ultrasound images." *Computerized Medical Imaging and Graphics*, vol. 24, pp. 221–229., 4 2000.

[13] K. Caballero, J. Barajas, O. Pujol, J. Mauri, and P. Radeva, "In-vivo IVUS tissue classification a comparison between normalized image reconstruction and RF signals analysis," in *Proc. 11^{th} Iberoamerican Congress on Pattern Recognition, Cancun, Mexico*, 2006, pp. 137–146.

[14] A. Nair, B. D. Kuban, E. M. Tuzcu, P. Schoenhagen, S. E. Nissen, and D. G. Vince, "Coronary plaque classification with intravascular ultrasound radiofrequency data analysis," *Circulation*, vol. 106, no. 17, pp. 2200–2206, October 2002.

[15] A. Nair, M. Margolis, B. Kuban, and D. Vince, "Automated coronary plaque characterisation with intravascular ultrasound backscatter: Ex vivo validation," *Eurointervention*, vol. 3, no. 1, pp. 113–120, 2007.

[16] L. Fellingham and F. Sommer, "Ultrasonic characterization of tissue structure in the in vivo human liver and spleen," *IEEE Transactions on Sonics and Ultrasonics*, vol. 31, no. 4, pp. 418–428, July 1984.

[17] F. Lizzi, M. Ostromogilsky, E. Feleppa, M. Rorke, and M. Yaremko, "Relationship of ultrasonic spectral parameters to features of tissue microstructure," *IEEE Transactions on Ultrasonics, Ferroelectrics and Frequency Control*, vol. 34, no. 3, pp. 319–329, May 1987.

[18] G. A. Rodriguez-Granillo, E. P. McFadden, M. Valgimigli, C. A. van Mieghem, E. Regar, P. J. de Feyter, and P. W. Serruys, "Coronary plaque composition of nonculprit lesions, assessed by in vivo intracoronary ultrasound radio frequency data analysis, is related to clinical presentation," *American Heart Journal*, vol. 151, no. 5, pp. 1020–1024, 2006.

[19] K. Nasu, E. Tsuchikane, O. Katoh, D. G. Vince, R. Virmani, J. F. Surmely, A. Murata, Y. Takeda, T. Ito, M. Ehara, T. Matsubara, M. Terashima, and T. Suzuki, "Accuracy of in vivo coronary plaque morphology assessment: A validation study of in vivo virtual histology compared with in vitro histopathology," *Journal of the American College of Cardiology*, vol. 47, no. 12, pp. 2405–2412, 2006.

[20] M. Kawasaki, H. Takatsu, T. Noda, Y. Ito, A. Kunishima, M. Arai, K. Nishigaki, G. Takemura, N. Morita, S. Minatoguchi, and H. Fujiwara, "Noninvasive quantitative tissue characterization and two-dimensional color-coded map of human atherosclerotic lesions using ultrasound integrated backscatter: comparison between histology and integrated backscatter images." *Journal of the American College of Cardiology*, vol. 38, no. 2, pp. 486–492, August 2001.

[21] M. Kawasaki, H. Takatsu, T. Noda, K. Sano, Y. Ito, K. Hayakawa, K. Tsuchiya, M. Arai, K. Nishigaki, G. Takemura, S. Minatoguchi, T. Fujiwara, and H. Fujiwara, "In vivo quantitative tissue characterization of human coronary arterial plaques by use of integrated backscatter intravascular ultrasound and comparison with angioscopic findings," *Circulation*, vol. 105, pp. 2487–2492, 2002.

[22] M. Kawasaki, B. Bouma, J. Bressner, S. Houser, S. Nadkarni, B. MacNeill, I. Jang, H. Fujiwara, and G. Tearney, "Diagnostic accuracy of optical coherence tomography and integrated backscatter intravascular ultrasound images for tissue characterization of human coronary plaques." *Journal of the American College of Cardiology*, vol. 48, no. 1, pp. 81–88, July 2006.

[23] S. O'Malley, M. Naghavi, and I. Kakadiaris, "One-class acoustic characterization applied to blood detection in IVUS," in *Proc. Medical Image Computing and Computer-Assisted Intervention*, Brisbane, Australia, 2007, pp. 202–209.

[24] A. Roodaki, A. Taki, S. K. Setarehdan, and N. Navab, "Modified wavelet transform features for characterizing different plaque types in IVUS images; a feasibility study," in *Proc. 9^{th} International Conference on Signal Processing. Beijing, China,*, October 2008, pp. 789–792.

[25] A. Katouzian, B. Baseri, E. E. Konofagou, and A. F. Laine, "An alternative approach to spectrum-based atherosclerotic plaque characterization techniques using intravascular ultrasound (IVUS) backscattered signals," in *Proc. 2^{nd} MICCAI Workshop on Computer Vision for Intravascular and Intracardiac Imaging. New York, USA*, 2008.

[26] A. Murashige, T. Hiro, T. Fujii, K. Imoto, T. Murata, Y. Fukumoto, and M. Matsuzaki, "Detection of lipid-laden atherosclerotic plaque by wavelet analysis of radiofrequency intravascular ultrasound signals: In vitro validation and preliminary in vivo application," *Journal of the American College of Cardiology*, vol. 45, no. 12, pp. 1954–60, 2005.

[27] A. Katouzian, B. Baseri, E. E. Konofagou, and A. F. Laine, "Automatic detection of blood versus non-blood regions on intravascular ultrasound (IVUS) images using wavelet packet signatures," in *Proc. Medical Imaging 2008: Ultrasonic Imaging and Signal Processing. San Diego, CA, USA*, February 2008.

[28] M. Papadogiorgaki, V. Mezaris, Y. Chatzizisis, G. Giannoglou, and I. Kompatsiaris, "Image analysis techniques for automated IVUS contour detection." *Ultrasound in Medicine and Biology*, vol. 34, no. 9, pp. 1482–1498, Sep. 2008.

[29] Z. Qi, W. Weiqi, M. Jianying, Q. Juying, and G. Junbo, "Contour extraction from IVUS images based on GVF snakes and wavelet transform," in *Proc. International Conference on Complex Medical Engineering, Beijing, China.*, 2007, pp. 536–541.

TABLE I

NUMBER OF EXAMPLES FROM CONTRAST AGENT (CA) AND BASELINE IVUS (BL) USED FOR TRAINING AND DEPLOYMENT FOR SEQUENCE 1.

Window size			Training		Deployment	
r	θ	t	CA	BL	CA	BL
255	13	13	18,924	9,055	9,462	4,528
255	13	7	17,949	13,844	8,975	6,921
255	13	5	20,474	16,610	10,238	8,305
255	7	13	14,838	8,473	7,419	4,236
255	7	7	20,165	15,270	10,082	7,634
255	7	5	22,959	18,218	11,479	9,109
255	5	13	15,394	8,693	7,697	4,346
255	5	7	20,912	15,762	10,456	7,881
255	5	5	23,791	18,836	11,896	9,419
127	13	13	27,968	11,570	13,984	5,785
127	13	7	26,046	17,474	13,022	8,737
127	13	5	29,505	20,829	14,753	10,415
127	7	13	21,501	10,665	10,751	5,333
127	7	7	28,754	19,136	14,377	9,568
127	7	5	32,513	22,709	16,256	11,355
127	5	13	31,873	13,636	15,937	6,818
127	5	7	42,713	24,487	21,356	12,243
127	5	5	33,551	23,348	16,775	11,675
63	13	13	33,679	13,041	16,839	6,520
63	13	7	44,922	23,504	22,461	11,752
63	13	5	50,790	27,922	25,396	13,961
63	7	13	36,912	14,306	18,456	7,153
63	7	7	49,196	25,606	24,598	12,803
63	7	5	38,616	25,295	19,308	12,648
63	5	13	38,019	15,267	19,010	7,633
63	5	7	50,689	27,330	25,344	13,664
63	5	5	39,730	25,972	19,865	12,987

TABLE II

NUMBER OF EXAMPLES FROM CONTRAST AGENT (CA) AND BASELINE IVUS (BL) USED FOR TRAINING AND DEPLOYMENT FOR SEQUENCE 2.

Window size			Training		Deployment	
r	θ	t	CA	BL	CA	BL
255	13	13	8,825	17,189	4,412	8,595
255	13	7	19,516	30,081	9,757	15,041
255	13	5	24,371	34,379	12,186	17,189
255	7	13	10,745	17,205	5,373	8,603
255	7	7	23,577	30,110	11,788	15,054
255	7	5	29,309	34,410	14,654	17,206
255	5	13	11,096	17,920	5,548	8,960
255	5	7	24,397	31,360	12,199	15,680
255	5	5	30,294	35,840	15,148	17,920
127	13	13	14,440	18,912	7,220	9,456
127	13	7	30,283	33,096	15,142	16,548
127	13	5	37,046	37,824	18,523	18,912
127	7	13	17,167	18,922	8,584	9,462
127	7	7	12,624	33,114	6,312	16,558
127	7	5	15,394	37,845	7,697	18,923
127	5	13	6,629	19,691	3,315	9,845
127	5	7	13,806	34,459	6,903	17,229
127	5	5	16,802	39,381	8,401	19,691
63	13	13	6,308	19,739	3,153	9,869
63	13	7	13,048	34,542	6,524	17,272
63	13	5	15,866	39,478	7,934	19,738
63	7	13	7,321	19,744	3,661	9,872
63	7	7	15,104	34,552	7,552	17,276
63	7	5	18,327	39,488	9,164	19,744
63	5	13	8,000	20,555	4,000	10,277
63	5	7	16,437	35,971	8,218	17,985
63	5	5	19,908	41,109	9,954	20,555

TABLE III

AVERAGE RATE OBTAINED FOR THE CLASSIFICATION OF CONTRAST AGENT (CA) AND BASELINE IVUS (BL) FOR CONTRAST DETECTION CLASSIFIERS 1 AND 2 (CDC_1 AND CDC_2 RESPECTIVELY) USING FREQUENCY-DOMAIN-BASED FEATURES.

Window size			CDC_1		CDC_2	
r	θ	t	CA(%)	BL(%)	CA(%)	BL(%)
255	13	13	94.87	96.85	93.29	93.16
255	13	7	96.47	90.05	92.47	96.63
255	13	5	96.35	82.05	82.80	96.59
255	7	13	96.62	95.68	97.83	96.69
255	7	7	96.61	82.48	85.16	96.74
255	7	5	73.24	81.01	74.58	96.65
255	5	13	91.77	96.36	96.54	96.37
255	5	7	95.15	82.28	82.55	96.60
255	5	5	50.23	94.76	71.57	96.54
127	13	13	93.79	95.24	92.22	95.08
127	13	7	96.65	80.72	86.04	96.45
127	13	5	73.32	78.87	76.05	96.73
127	7	13	96.43	88.83	93.28	96.74
127	7	7	70.08	87.48	75.72	93.80
127	7	5	70.25	81.69	66.17	93.39
127	5	13	93.32	85.04	87.63	90.66
127	5	7	90.54	75.82	73.37	91.05
127	5	5	70.26	80.44	63.40	93.55
63	13	13	91.85	86.96	91.04	90.62
63	13	7	90.83	78.62	79.36	91.21
63	13	5	90.79	72.45	72.36	90.80
63	7	13	90.96	83.45	85.31	90.56
63	7	7	91.12	70.14	72.59	90.84
63	7	5	70.15	75.63	60.19	93.74
63	5	13	90.90	80.42	82.68	90.56
63	5	7	91.09	64.14	69.72	91.22
63	5	5	70.39	72.03	69.30	88.94

TABLE IV

AVERAGE RATE OBTAINED FOR THE CLASSIFICATION OF CONTRAST AGENT (CA) AND BASELINE IVUS (BL) FOR CONTRAST DETECTION CLASSIFIERS 1 AND 2 (CDC_1 AND CDC_2 RESPECTIVELY) USING WAVELET-BASED FEATURES.

Window size			CDC_1		CDC_2	
r	θ	t	CA(%)	BL(%)	CA(%)	BL(%)
255	13	13	91.23	94.14	98.62	95.38
255	13	7	96.82	93.29	97.31	96.94
255	13	5	96.70	91.85	94.69	96.81
255	7	13	96.80	94.14	98.51	96.95
255	7	7	96.86	93.04	96.46	96.79
255	7	5	96.87	90.05	93.93	96.57
255	5	13	96.44	94.25	95.63	93.78
255	5	7	96.89	92.69	96.05	96.64
255	5	5	96.82	89.69	93.03	96.55
127	13	13	94.02	91.50	97.17	94.04
127	13	7	96.62	89.15	93.98	96.60
127	13	5	96.79	86.03	90.74	96.72
127	7	13	96.66	91.94	96.44	96.62
127	7	7	93.95	75.13	90.14	97.24
127	7	5	93.78	69.51	88.85	94.34
127	5	13	90.88	77.22	92.01	95.86
127	5	7	90.63	58.86	88.36	94.58
127	5	5	94.02	70.38	86.10	95.73
63	13	13	90.62	70.50	94.44	93.26
63	13	7	90.49	55.90	90.91	93.52
63	13	5	90.86	51.16	86.57	92.68
63	7	13	91.34	62.77	92.31	94.83
63	7	7	91.29	55.03	88.00	94.49
63	7	5	93.65	62.35	83.22	96.09
63	5	13	91.05	64.52	90.86	94.87
63	5	7	90.80	55.93	86.77	93.37
63	5	5	92.37	64.13	81.19	96.41